25-29 August 2024
inter.noise
NANTES FRANCE

Sound absorbers from waste walnut shells

Keith Attenborough[1]
The Open University
Walton hall, Milton Keynes, MK7 6AA, UK

Mohammad Javad SheikhMozafari [2]
Tehran University of Medical Sciences,
Tehran, Iran

Ebrahim Taban[3]
Mashhad University of Medical Sciences
Mashhad, Iran

Leila Tajik, Samira Rasaneh and Mohammad Faridan
Lorestan University of Medical Sciences,
Khorramabad,
Iran

ABSTRACT

Waste walnut shells have been cleaned, dried, chopped, glued, pressed, and molded to form porous cylinders for measurement of normal incidence sound absorption coefficient spectra in an impedance tube. Porosities and flow resistivities have been measured non-acoustically. Field Emission Scanning Electron Microscopy images, used to obtain fragment size for determining shell density, reveal that the fragment surfaces are rough, which may influence acoustical performance. Measured absorption spectra have been compared with predictions of two analytical models for acoustical properties of rigid porous media, which assume microstructures of identical uniform parallel slanted slits (SS) and non-uniform cylindrical pores with a log normal radius distribution (NUPSD) respectively. Measured values of flow resistivity and porosity are used in the models but tortuosity is adjusted to give best agreement with the quarter wavelength resonance in the measured absorption coefficient spectra. Predictions agree best with data for samples made from the smallest shell fragments. These samples have the highest values of tortuosity, flow resistivity and offer good absorption at speech frequencies which suggests that recyclable and sustainable sound absorbers made from walnut shell wastes could be useful for controlling indoor reverberation.

[1] Keith.Attenborough@open.ac.uk
[2] Mj-sheikhmozafari@razi.tums.ac.ir
[3] Tabane@mums.ac.ir

1. INTRODUCTION

Porous materials made from synthetic fibers offer effective sound absorption, good heat insulation, and high mechanical strength. But they are not biodegradable. Disposing of these materials can cause undesirable environmental problems. For example, toxic gases are released when they are incinerated. Moreover, their production involves high energy consumption and results in emissions of carbon dioxide, methane, and nitrous oxide into the atmosphere. There is increasing interest in creating sound absorbing materials from naturally occurring granular or fibrous sources. Not only are such materials biodegradable, but they can have lower density, higher electrical resistance, better specific strength, cost-effectiveness, and they are non-toxic [1,2].

Many naturally occurring fibers can be used to create good sound absorbers, but, while they offer useful absorption at middle and high frequencies, they are less effective below 500 Hz and improving their low frequency absorption by increasing thickness might not be practical or cost-effective. Also, fibrous sound absorbers are not appropriate in environments requiring clean and cleanable surfaces, such as restaurants, clean rooms, and hospitals. In households, the dispersion of fibers contributes to air pollution and exacerbates respiratory problems. Furthermore, fibrous sound absorbers are not robust and are susceptible to dust, rainfall, and extreme temperatures. More durable sound absorbers can be made from granular wastes, for example from fruit stones [3,4] and pistachio shells [5]. This paper reports a procedure for manufacturing porous samples from waste walnut shells and measurements of their normal incidence sound absorption coefficients, porosity, and flow resistivity. Although direct measurement of sound absorption coefficients is preferred, it is subject to constraints such as high costs, limited equipment accessibility, and the need for specialist facilities. Mathematical models can provide alternative ways for estimating the acoustic absorption properties. Ideally these models should involve as few parameters as possible. The capabilities of two models for the acoustical properties of rigid porous materials to predict the measured absorption spectra of the walnut shell samples have been investigated. The models are for identical uniform parallel slanted slit pores (SS) and a log normal size distribution of cylindrical pores (NUPSD).

2. SAMPLE FABRICATION AND CHARACTERISATION

2.1. The fabrication process

Waste walnut shells from industry and households were cleaned with distilled water to eliminate impurities and dirt and treated with boric acid to enhance resistance against fungal growth, insect attacks, and enzymatic activities. The shells were dried at 70°C in an oven for 24 hours then chopped to three different extents (minimal, moderate and extensive), and mixed with a polyvinyl alcohol (PVA) adhesive which was selected for its environmental compatibility and ability to dissolve in water. The potential influence of the PVA on acoustical performance was reduced by using as little as necessary to achieve structural integrity. The required amount of adhesive was one-third of the weight of samples made from shell fragments after moderate and extensive chopping and one-half of the weight of samples made after minimal chopping. Cylindrical samples with a diameter of 10 cm corresponding to that of the impedance tube sample holder and with four different thicknesses (20, 40, 60 and 80 mm) were made by filling aluminum and polypropylene molds with the shell fragment mix and applying pressure.

The stages in the fabrication procedure are shown in Figure 1 which includes examples of samples composed of the shell fragments resulting from the three degrees of chopping.

Figure 1: Sample preparation.

2.2. Thickness and bulk density

The thickness was measured ten times at various positions across each sample and the average for each sample is listed in Table 1. The bulk density was determined by weighing each sample three times and taking the average. The average values are shown in Table 1.

2.3. SEM Imaging

The surfaces of the walnut shell fragments were subjected to gold sputtering and imaged using MIRA3 TESCAN FE-SEM equipment [6]. Figure 2 shows images of fragments resulting from each of the different degrees of chopping. The roughness of the shell fragment surfaces affects airflow resistivity and tortuosity, and thereby the quarter-wavelength resonance peaks in the absorption spectra of hard backed samples.

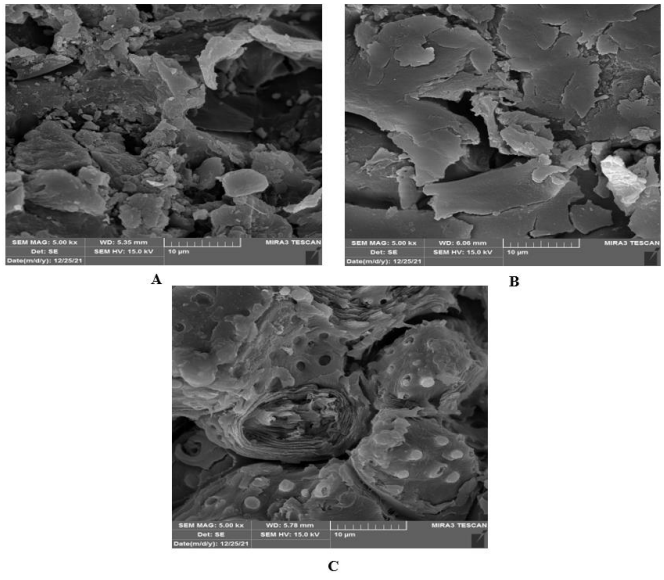

Figure 2: FE-SEM images of walnut shell fragments from each degree of chopping.

2.4. Sound absorption

Normal incidence sound absorption coefficient (SAC) spectra were measured in a large impedance tube (BSWA SW422, BSWA Technology Co., Ltd.) using the transfer function method [7]. The measurement system included a loudspeaker, PA50 amplifier, data acquisition system, two 1/4-inch condenser microphones (MPA416 type), VA-Lab software, and associated components. Prior to these measurements, the microphones were calibrated using a BSWA calibrator at 1 kHz and a sound pressure level (SPL) of 114 dB. Tests were conducted under controlled conditions viz. temperature 20 ± 2 °C, relative humidity 45 ± 5%, and atmospheric pressure 1.01325×10^5 Pa. The measurement of the SAC spectrum for each sample was made on three occasions, being repeated four times on each occasion, and the average was recorded.

2.5. Porosity

The porosity (∅**)** of connected air-filled pores in each sample is given by Equation (1)

$$\emptyset = \mathbf{1} - \frac{\rho_b}{\rho_m} \tag{1}$$

where ρ_b is the bulk density and ρ_m is the density of the walnut shells.

The weights of ten shell fragments were averaged. The radius of a cylindrical volume equivalent to that of a shell fragment was obtained from the corresponding FESEM image and the height of the equivalent cylinder was taken to be the length of the fragment measured with calipers. The shell fragment weight divided by the volume of its equivalent cylinder was taken to be the walnut shell density. Values of porosity are listed in Table 1.

Table 1: Measured and fitted parameters.

Sample	Thickness (mm)	Weight (g)	Bulk density (kg m^{-3})	Flow resistivity (Nm^{-4}s)	Porosity (%)	Tortuosity
Minimally chopped	20	72	458(±10)	4890(±130)	58.60	1.217
	40	137	438(±15)	4460 (±87)	58.15	1.217
	60	221	469(±18)	4079(±108)	57.70	1.217
	80	271	431(±17)	3760(±133)	57.35	1.217
Moderately chopped	20	92	585(±23)	5240(±145)	60.75	1.700
	40	165	524(±19)	4905(±109)	60.30	2.420
	60	252	534(±16)	4630 (±98)	59.95	1.333
	80	335	535(±22)	4390(±139)	59.60	1.132
Extensively chopped	20	100	638(±29)	5670(±125)	61.90	2.420
	40	183	585(±33)	5405(±103)	61.45	2.420
	60	292	620(±21)	5180(±147)	61.15	2.420
	80	359	571(±19)	5009(±138)	60.75	2.000

2.6. Flow resistivity

The airflow resistivity (σ) of each sample was measured using a standard method [8]. A

schematic of the airflow resistivity measurements is given elsewhere [5]. There were three repetitions of the flow resistivity measurements and Table 1 shows the averaged results.

3. THREE-PARAMETER MODELS FOR PREDICTING SOUND ABSORPTION

3.1. Identical uniform parallel slanted slits (SS)

The expressions for the complex density $\rho(\omega)$ and complex compressibility $C(\omega)$ within a uniform pore of any shape are [9]:

$$\rho(\omega) = \rho_0/H(\lambda), \quad C(\omega) = \left[\gamma - (\gamma - 1)H\left(\lambda\sqrt{N_{Pr}}\right)\right] \tag{2}$$

where time-dependence $e^{-i\omega t}$ is understood, ω is angular frequency, λ is a dimensionless parameter, $(\gamma P_0)^{-1} = (\rho_0 {c_0}^2)^{-1}$ represents the inverse of the adiabatic compressibility of air, and γ, P_0, N_{pr} are the specific heat ratio, atmospheric pressure, and Prandtl number, respectively.

For a parallel sided slit of width $2b$, $\lambda = b\sqrt{\omega/\nu}$, $\nu = \mu/\rho_0$, μ is the dynamic coefficient of viscosity, and ρ_0 is the density of air and

$$H(\lambda) = 1 - \tanh\left[\lambda\sqrt{(-i)}\right]/\lambda\sqrt{(-i)} \tag{3}$$

The relationship between the flow resistivity σ, tortuosity α_∞ and porosity ϕ of a porous medium in which the pores of are identical slits inclined at angle ϑ to the surface normal is

$$\sigma = 3\mu\alpha_\infty/\phi b^2, \quad \alpha_\infty = 1/(\cos\vartheta)^2 \tag{4}$$

The bulk propagation constant $k(\omega)$, relative characteristic impedance $Z_C(\omega)$, surface impedance $Z(d)$, reflection coefficient $R(d)$ and absorption coefficient $\alpha(d)$ of a rigid porous hard backed layer of thickness d in which the pores are parallel slanted slits of width $2b$ and their edge to edge spacing is $b(1-\phi)/\phi$, are given by equations (5) and (6).

$$k(\omega) = \omega\sqrt{\alpha_\infty \rho(\omega) C(\omega)}, \quad Z_C(\omega) = (\rho_0 c_0)^{-1}\sqrt{(\alpha_\infty/\phi^2)\,\rho(\omega)/C(\omega)} \tag{5}$$

$$Z(d) = Z_C(\omega)\coth(-ik(\omega)d), R(d) = \frac{\rho_0 c_0 - Z(d)}{\rho_0 c_0 + Z(d)}, \alpha(d) = 1 - \left|\left(R(d)\right)^2\right| \tag{6}$$

In the absence of an independent measurement of tortuosity, its value can be estimated by substituting measured values of flow resistivity and porosity and fitting the absorption coefficient data.

3.2. Non uniform pore size distribution (NUPSD)

A model for the acoustical properties of a medium containing non-uniform cylindrical pores with a log-normal radius distribution [10,11] introduces a Padé approximation for the bulk complex density,

$$\rho_b(\omega) = (\alpha_\infty/\phi)\left[1 + F_\rho(\varepsilon_\rho)/(\varepsilon_\rho{}^2)\right], \quad F_\rho(\varepsilon) = \frac{1+a_{\rho1}\varepsilon_\rho+a_{\rho2}\varepsilon_\rho{}^2}{1+b_{\rho1}\varepsilon_\rho} \tag{7}$$

where $\varepsilon_\rho = \sqrt{\left(\frac{-i\omega\rho_0\alpha_\infty}{\phi\sigma}\right)}$, $a_{\rho1} = \theta_{\rho1}/\theta_{\rho2}, a_{\rho2} = \theta_{\rho1}$, $b_{\rho1} = a_{\rho1}, \theta_1 = \frac{1}{3}, \theta_{\rho2} = e^{-\frac{1}{2}(\beta \log 2)^2}$, and β is the standard deviation of the pore size distribution in φ units such that a pore dimension in mm $= 2^{-\varphi}$.

The corresponding Padé approximation for bulk compressibility is

$$C_b(\omega) = \left[\gamma - (\gamma-1)/\left(1 + F_C(\varepsilon_C)/(\varepsilon_C{}^2)\right)\right], \; F_C(\varepsilon) = \frac{1+a_{C1}\varepsilon_C+a_{C2}\varepsilon_C{}^2}{1+b_{C1}\varepsilon_C} \tag{8}$$

where $\varepsilon_C = \sqrt{\left(\frac{-i\omega\rho_0\alpha_\infty N_{Pr}}{\phi\sigma'}\right)}$, $a_{C1} = \theta_{C1}/\theta_{C2}$, $a_{C2} = \theta_{C1}$, $b_{C1} = a_{C1}$, $\theta_{C1} = \frac{1}{3}$, $\theta_{C2} = e^{-\frac{3}{2}(\beta \log 2)^2}/\sqrt{2}$ and $\sigma' = [\frac{8\mu}{\phi \bar{r}^2}]e^{-6(\beta \log 2)^2}$.

When a measurement of the pore size distribution is not available, a value of standard deviation can be estimated from a value of tortuosity by using equation (9) [10,11],

$$\alpha_\infty = e^{4(\beta \log 2)^2} . \tag{9}$$

4. SOUND ABSORPTION COEFFICENT (SAC) SPECTRA

4.1. The influence of sample thickness

Figure 3 shows the influence of thickness on the SAC spectra for shell fragment sizes resulting from each of the three degrees of chopping. As is expected of the quarter wavelength resonances of hard backed low flow resistivity porous layers, the absorption peak moves to lower frequency with increasing thickness. Also, for a given thickness the sound absorption increases as the size of shell fragments from which the samples are composed decreases.

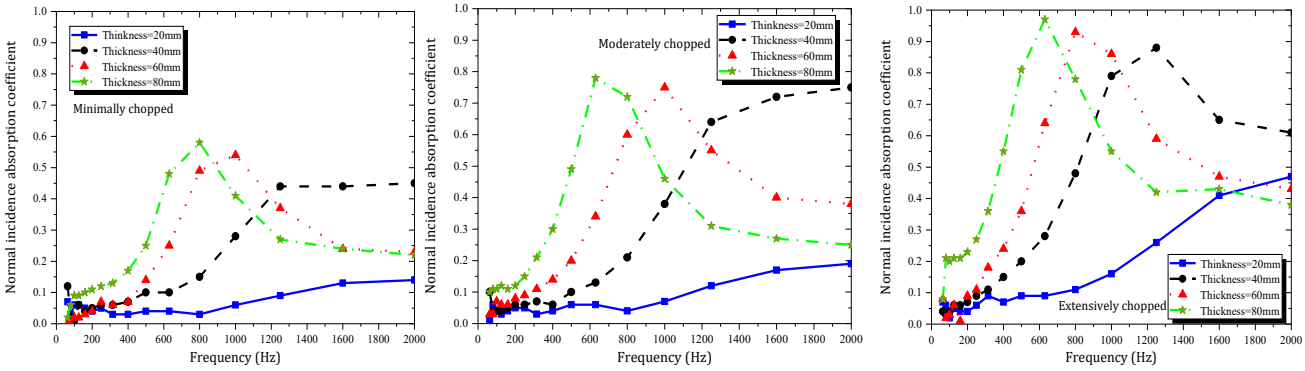

Figure 3: The effect of thickness on the sound absorption coefficient for samples made from the shell fragments resulting from each degree of chopping.

4.2. The influence of shell fragment size

Figure 3 indicates that the absorption peaks and overall absorption are increased as the shell fragment size decreases. The values in Table 2, show how the shell fragment size influences the mean bulk density, air flow resistivity and tortuosity. The influence of bulk density on the measured absorption spectra is shown for 40 mm and 80 mm thick samples in

Figure 4. Overall, the absorption increases with density. However, as indicated above 1.2 kHz in Figure 4(a), and, as has been shown elsewhere [12,13], increasing density does not increase absorption indefinitely.

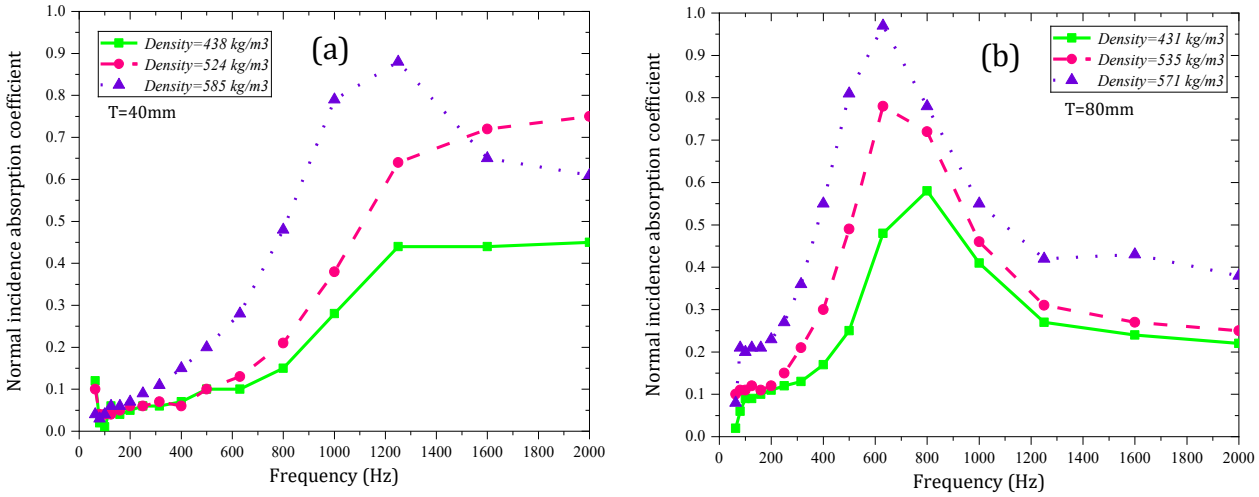

Figure 4: The effect of bulk density on the sound absorption coefficient for (a) 40 mm and (b) 80 mm thick samples.

The influence of shell fragment size is illustrated further in Figures 5(a) and (b). The higher mean flow resistivity and tortuosity of the samples composed from the smaller shell fragments causes the magnitude of the peak in the SAC spectra to increase and shift to lower frequencies. This is due in part to the increase in tortuosity with decreasing particle size, as has been observed in other studies [14,15].

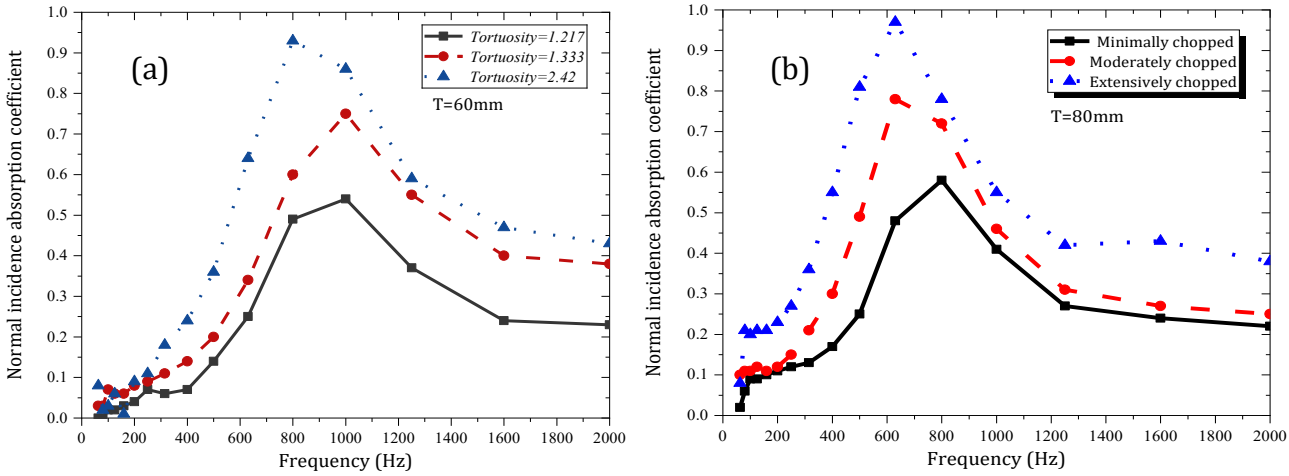

Figure 5: The effect of shell fragment size on the sound absorption coefficient for (a) 60 mm and (b) 80 mm thick samples.

5. COMPARISONS BETWEEN PREDICTIONS AND DATA

Measured and predicted SAC spectra are compared in Figure 6 and the associated parameter values are listed in Table 3. The tortuosity required for the SS model predictions have been obtained by choosing values to fit the absorption peak frequency for each sample. The standard deviation of the log normal pores size distribution required for the NUPSD model has been obtained from this fitted tortuosity by using equation (12).

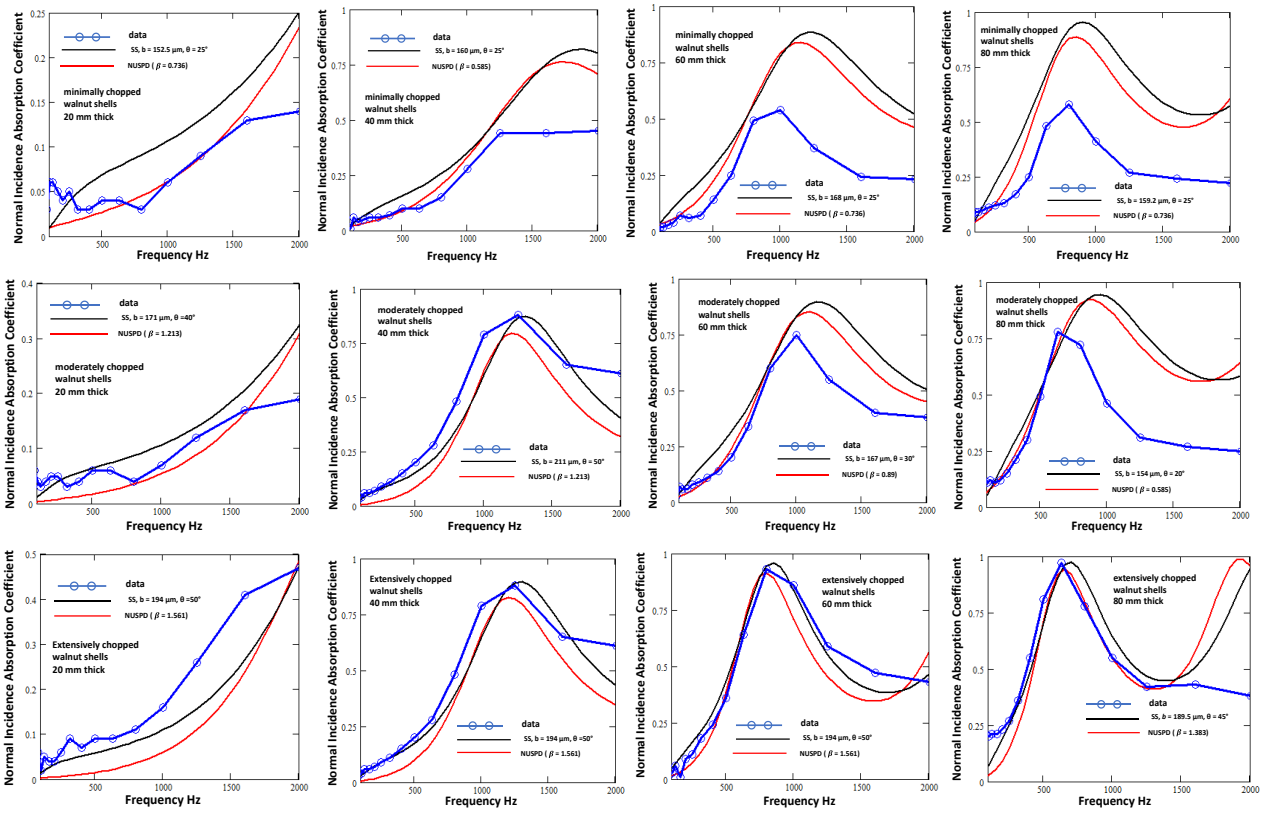

Figure 6: Comparisons of predicted and measured normal incidence sound absorption spectra.

There are systematic discrepancies since the data are for third octave bands, whereas the predictions are for 50 Hz intervals. Furthermore, there may be losses in the measurement system not accounted for in the models. However, except for the thicker samples made from larger shell fragments, the agreement between predictions of both models and SAC data is reasonable. Moreover, the agreement improves as the shell fragment size in the samples decreases. Overall, there is little to choose between the prediction capabilities of the two models. The usefulness of these three parameter models in comparison with the JCA and JCAL models, which require estimated values of an additional two and three parameters respectively, has been demonstrated also in modelling the sound absorption of samples made from wood chips [16].

6. CONCLUSIONS

The acoustical properties of samples composed of glued walnut shell fragments with sizes corresponding to shells chopped to three extents have been investigated. The surface and particle size characteristics of the shell fragments were investigated using Field Emission Scanning Electron Microscopy. Measurements were made of their normal incidence absorption coefficient spectra were measured in an impedance tube and non-acoustical measurements of their porosity and flow resistivity were made. The FESEM images showed that the surfaces of the shell fragments are rough. Increasing thickness increased the peak and overall absorption and shifted the peaks to lower frequencies. The samples made from the smallest fragments offered the highest absorption for a given thickness and had the highest bulk density, flow resistivity and fitted tortuosity. The measured absorption spectra were compared with predictions of models assuming either identical slanted slit pores or a non-uniform size distribution of cylindrical pores. The best agreement of predictions with

data was observed for the samples composed from the smallest fragments. The 0.04 cm and 0.06 m thick hard backed samples have useful sound absorption between 800 Hz and 1.5 kHz. This suggests that walnut shell wastes offer a sustainable source for manufacturing recyclable sound absorbers and controlling reverberation at speech frequencies in indoor environments.

Table 3: Values of parameters used in the SS and NUPSD models.

Degree of chopping	***d* mm**	**Slit width mm**	***θ*°**	***β* φ-units**
Minimal	20	0.318	25	0.736
	40	0.320	25	0.736
	60	0.336	25	0.736
	80	0.318	25	0.736
Moderate	20	0.346	40	1.213
	40	0.422	50	1.561
	60	0.334	30	0.890
	80	0.308	20	0.585
Extensive	20	0.388	50	1.561
	40	0.388	50	1.561
	60	0.388	50	1.561
	80	0.380	45	1.383

REFERENCES

1. J. P. Arenas, R. del Rey, J. Alba and R. Oltra. Sound-absorption properties of materials made of esparto grass fibers. **Sustainability**, **12(14)**, 5533, 2020.
2. F. Valipour, E. Taban, S. E. Samaei, G. Pourtaghi and Z. N. Konjin. Improvement of natural fiber's properties and evaluation of its applicability as eco-friendly materials in noise pollution control. **Journal of Environmental Health Science and Engineering**, **20(2)**, 647 – 656, 2022.
3. J. G. Borrell, E. J. Sanchis, J. S. Alcaraz and I. M. Belda. Sustainable sound absorbers from fruit stones waste. **Applied Acoustics**. **161**, 107174, 2020.
4. M. J. SheikhMozafari, E. Taban, P. Soltani, M. Faridan and A. Khavani. Sound absorption and thermal insulation performance of sustainable fruit stone panels. **Applied Acoustics**, **217**, 109836, 2024.
5. N. Hemmati, M. J. Sheikhmozafari, E. Taban, L. Tajik and M. Faridan. Pistachio shell waste as a sustainable sound absorber: an experimental and empirical investigation. **International Journal of Environmental Science and Technology 21**, 4867–4880, 2024.
6. S. E. Samaei, H. A. Mahabadi, S. M. Mousavi, A. Khavanin, M. Faridan and E. Taban. The influence of alkaline treatment on acoustical, morphological, tensile and thermal properties of Kenaf natural fibers. **Journal of Industrial Textiles**, **51(5_suppl)**, 8601S-25, 2022.

7. ISO10534-2:2003 Determination of sound absorption coefficient and impedance in impedance tubes Part 2: Transfer-function method.
8. ISO 9053:2019 Determination of airflow resistance Part 1: Static airflow method.
9. M. R. Stinson. The propagation of plane sound waves in narrow and wide circular tubes, and generalization to uniform tubes of arbitrary cross-sectional shape. **The Journal of the Acoustical Society of America. 89(2)**, 550 – 558, 1991.
10. K. V. Horoshenkov, Groby J-P, Dazel O. Asymptotic limits of some models for sound propagation in porous media and the assignment of the pore characteristic lengths. The journal of the acoustical society of America. 2016;139(5):2463-74
11. F. Saati, K-A. Hoppe, S. Marburg and K. V. Horoshenkov. The accuracy of some models to predict the acoustical properties of granular media, **Applied Acoustics, 185**, 108358, 2022.
12. E. Taban, P. Soltani, U. Berardi, A. Putra, S. M. Mousavi and M. Faridan. Measurement, modeling, and optimization of sound absorption performance of Kenaf fibers for building applications. **Building and Environment**, **180**, 107087. 2020.
13. S. Mehrzad, E. Taban, P. Soltani, S. E. Samaei and A. Khavanin. Sugarcane bagasse waste fibers as novel thermal insulation and sound-absorbing materials for application in sustainable buildings. **Building and Environment**. **211**, 108753, 2022.
14. S. Prabhune, Y. Munde, A. Shinde and I. Siva. Appraising the acoustic performance and related factors of natural fiber: A review. **Journal of Natural Fibers**. **19(16)**, 13475-94, 2022.
15. M. Nordin, L. Wan, M. Zainulabidin, A. Kassim and A. Aripin. Research finding in natural fibers sound absorbing material. **ARPN Journal of Engineering and Applied Sciences**. **11(14)**, 79 – 85, 2016.
16. M. Lashgari, E. Taban, M. J. SheikhMozafari, P. Soltani, K. Attenborough and A. Khavanin, Wood chip sound absorbers: measurements and models, **Applied Acoustics**, **230**, 109963, 2024.